

Vibrational Resonance in a System with a Signum Nonlinearity

K. Abirami¹, S. Rajasekar^{1,†}, M.A.F. Sanjuan²

¹School of Physics, Bharathidasan University, Tiruchirapalli 620 024, Tamilnadu, India

²Departamento de Física, Universidad Rey Juan Carlos, Tulipán s/n, 28933 Móstoles, Madrid, Spain

Submission Info

Communicated by Referees
 Received DAY MON YEAR
 Accepted DAY MON YEAR
 Available online DAY MON YEAR

Keywords

Vibrational resonance
 Signum nonlinearity
 Biharmonic force

Abstract

We present our investigation on vibrational resonance in a system with a signum nonlinearity. We construct an exact analytical solution of the system in the presence of an external biharmonic force with two frequencies ω and Ω , $\Omega \gg \omega$ and use it for the computation of the response amplitude Q at the low-frequency ω . We analyse the effect of the strength of the signum nonlinearity on vibrational resonance for the cases of the potential with a single-well, a double-well and a single-well with a double-hump. An interesting feature of vibrational resonance in the system is that Q does not decay to zero for g (the amplitude of the high-frequency force) $\rightarrow \infty$. We compare the features of the vibrational resonance of these two systems, since the potential of the system with the signum nonlinearity and that of the Duffing oscillator show similar forms. The strength of the nonlinearity in these two systems is found to give rise distinct effects on resonance.

©2014 L&H Scientific Publishing, LLC. All rights reserved.

1 Introduction

Nonlinear systems are capable of showing a rich variety of fascinating dynamics. Nonlinearity can arise from the dissipative force or from the restoring force. In the ubiquitous Duffing oscillator [1, 2], the dissipative force is linear while the restoring force has a cubic nonlinearity. In the van der Pol oscillator, the dissipative force is nonlinear and the restoring force is linear [2]. There is another class of nonlinear systems where the nonlinear function is piecewise linear [3–5]. An extensively studied piecewise linear system is the Chua's circuit [3–6], in which the nonlinear circuit element is Chua's diode and its characteristic function is a piecewise linear function. An interesting feature of nonlinear systems with a piecewise linear function as the only nonlinearity is that, in general, it is possible to construct an exact analytical solution even for chaotic systems. The dynamics of many piecewise linear systems with more than two linear regions have been investigated in detail [7–12].

A simple nonlinearity can be a piecewise linear function, for example the signum function $\text{sgn}(x)$, where $\text{sgn}(x) = 1$ for $x > 0$ and -1 for $x < 0$ and $|x|$. Such nonlinearities are found to arise in certain real systems [13–22]. The potential $V(x) = \frac{1}{2}\omega_0^2 x^2 + \beta|x|$ admits all the four forms of the potential $V(x) = \frac{1}{2}\omega_0^2 x^2 + \frac{1}{4}\beta x^4$ of the Duffing oscillator, an ubiquitous and a prototype nonlinear oscillator. A periodically driven system with a signum nonlinearity is found to show period doubling route to chaos and an onion-like chaotic attractor [19].

[†]Corresponding author.

Email address: nk.abirami@gmail.com, rajasekar@cndd.bdu.ac.in, miguel.sanjuan@urjc.es

The prime goal of the present paper is to construct an exact analytical solution of a system with the signum nonlinearity $\text{sgn}(x)$ and driven by a biharmonic force and investigate the vibrational resonance phenomenon through its analytical solution. Vibrational resonance [23] is a nonlinear resonant behaviour induced at the low-frequency ω of the input periodic signal by a high-frequency ($\Omega \gg \omega$) periodic force. The occurrence of vibrational resonance has been studied in certain nonlinear continuous time dynamical systems [23–37] and maps [38, 39] with smooth nonlinearities. For systems with polynomial type potentials, using the theoretical method proposed by Blekhman and Landa [26], an analytical approximate expression for response amplitude Q at the low-frequency ω can be obtained. Using this expression for Q the features of vibrational resonance have been studied in certain nonlinear systems.

The paper is organized as follows. In sec. 2 we construct the exact analytical solution of the system with the signum nonlinearity $\text{sgn}(x)$ and driven by a biharmonic force $F(t) = f \cos \omega t + g \cos \Omega t$, $\Omega \gg \omega$. We present the solution separately for the underdamped, critically damped and overdamped cases. We analyse the contribution of various terms in the analytical solution on the response amplitude $Q(\omega)$. Then consider the system with single-well potential in sec. 3. We show the occurrence of vibrational resonance by varying the control parameter g and explain the mechanism of resonance in terms of the resonant frequency of the system. Next, we point out the influence of strength β of the nonlinear term on the value of g at which resonance occurs (denoted as g_{VR}), the value of Q at resonance (denoted as Q_{max}) and the value of Q in the limit of $g \rightarrow \infty$ (denoted as Q_{L}). The vibrational resonance of the system will be compared with the single-well Duffing oscillator. Section 4 is devoted to the signum nonlinear system with a double-hump single-well potential. The parameter β has a strong influence on vibrational resonance. Depending upon the value of β the system displays no resonance, a single resonance and a double resonance. We distinguish the vibrational resonance of the signum nonlinear system with that of the Duffing oscillator with double-hump single-well potential. The features of vibrational resonance in the signum nonlinear system with double-well potential is presented in sec. 5. Section 6 contains the conclusions.

2 The Biharmonically Driven Oscillator with a Signum Nonlinearity

The equation of motion of a biharmonically driven system with the signum nonlinearity is given by

$$\ddot{x} + d\dot{x} + \omega_0^2 x + \beta \text{sgn}(x) = f \cos \omega t + g \cos \Omega t, \quad \Omega \gg \omega \quad (1)$$

where d is the damping coefficient, ω_0^2 is the natural frequency of the system, β is the strength of the signum nonlinearity and $\text{sgn}(x)$ is the signum function. In the system (1) $f \cos \omega t$ and $g \cos \Omega t$ are two input signals with high-frequency Ω and low-frequency ω and g and f are the strengths or amplitudes of these signals, respectively.

The potential of the system (1) in absence of the damping and external periodic forces is

$$V_S = \frac{1}{2} \omega_0^2 x^2 + \beta |x|. \quad (2)$$

The potential of the well-known Duffing oscillator is

$$V_D = \frac{1}{2} \omega_0^2 x^2 + \frac{1}{4} \beta x^4. \quad (3)$$

The shapes of the potentials V_S and V_D depend on the parameters ω_0^2 and β . Table 1 summarizes the conditions on ω_0^2 and β for each of the four shapes of the potentials V_S and V_D . Note that V_S is of a double-well form for $\omega_0^2 > 0$, $\beta < 0$ while for this choice of the parameters V_D is of a single-well with a double-hump shape. For $\omega_0^2 < 0$ and $\beta > 0$ the shape of V_S is of a single-well with a double-hump while that of V_D is of a double-well. The point is that V_S mimics all the four forms of the potential V_D . Figure 1 depicts the four forms of the potential functions V_S and V_D . The inverted potential is physically uninteresting, since $x(t) \rightarrow \pm\infty$ for all

Table 1 Sign of ω_0^2 and β and the corresponding shape of the Duffing oscillator and the signum oscillator. In this table CC and DC refer to continuous curve and dashed curve, respectively.

Sign of		Shape of the Potential of	
ω_0^2	β	Duffing oscillator	Signum oscillator
+	+	Single-well (DC in Fig. 1(a))	Single-well (CC in Fig. 1(a))
-	+	Double-well (DC in Fig. 1(b))	Single-well with a double-hump (CC in Fig. 1(b))
+	-	Single-well with a double-hump (DC in Fig. 1(c))	Double-well (CC in Fig. 1(c))
-	-	Inverted single-well (DC in Fig. 1(d))	Inverted single-well (CC in Fig. 1(d))

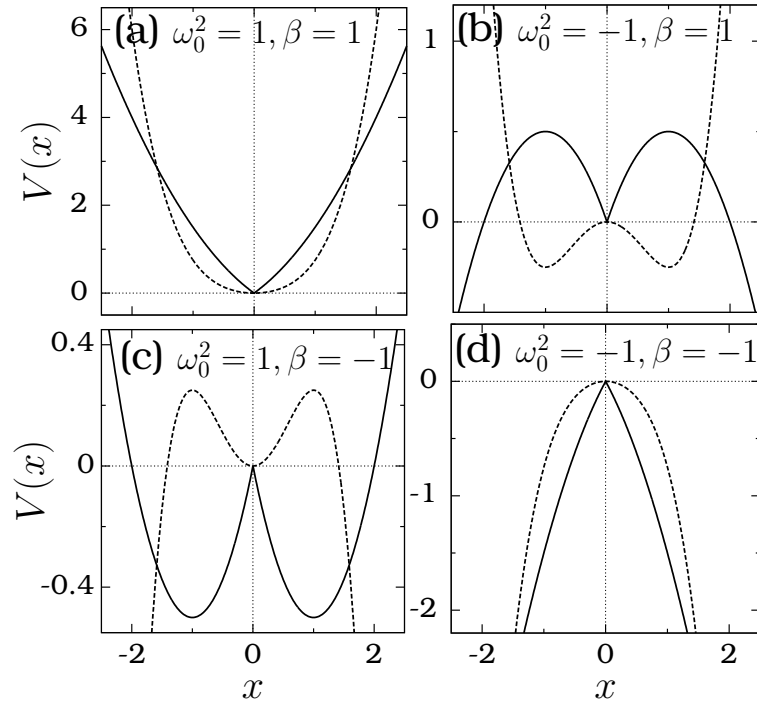


Fig. 1 Shapes of the potentials V_S and V_D for some selective values of ω_0^2 and β . In all the subplots, the continuous and the dashed curves represent V_S and V_D , respectively.

initial conditions of the periodically driven system. We construct the exact analytical solution and analyse the vibrational resonance separately for the other three forms of the potential V_S . Also, we compare the resonance dynamics of the system (1) with that of the Duffing oscillator.

2.1 Analytical Solution

In order to construct the general solution of Eq. (1), we rewrite it with $x = x_+$ for $x \geq 0$ and $x = x_-$ for $x < 0$ as

$$\ddot{x}_+ + d\dot{x}_+ + \omega_0^2 x_+ = f \cos \omega t + g \cos \Omega t - \beta, \text{ for } x_+ \geq 0 \tag{4a}$$

$$\ddot{x}_- + d\dot{x}_- + \omega_0^2 x_- = f \cos \omega t + g \cos \Omega t + \beta, \text{ for } x_- < 0. \tag{4b}$$

As the Eqs. (4a) and (4b) are linear in x_+ and x_- , respectively, and are constant coefficients equations, their solutions can be written separately for the regions $x_+ \geq 0$ and $x_- < 0$ and matching the two solutions at $x = 0$. The solutions are written separately for the three cases $d^2 > 4\omega_0^2$, $d^2 = 4\omega_0^2$ and $d^2 < 4\omega_0^2$.

Case 1: Overdamping – $d^2 > 4\omega_0^2$

For the overdamping case, we have obtained the solution as

$$x_{\pm}(t) = A_{\pm}e^{\lambda_{\pm}t} + B_{\pm}e^{-\lambda_{\pm}t} + F_1 \sin \omega t + F_2 \cos \omega t + G_1 \sin \Omega t + G_2 \cos \Omega t \mp \frac{\beta}{\omega_0^2}, \quad (5a)$$

where

$$A_{\pm} = \frac{e^{-\lambda_{\pm}t_0}}{\lambda_{+} - \lambda_{-}} \left[\dot{x}_0 - \lambda_{-}x_0 + (\lambda_{-}F_1 + \omega F_2) \sin \omega t_0 + (\lambda_{-}F_2 - \omega F_1) \cos \omega t_0 + (\lambda_{-}G_1 + \Omega G_2) \sin \Omega t_0 + (\lambda_{-}G_2 - \Omega G_1) \cos \Omega t_0 \mp \lambda_{-} \frac{\beta}{\omega_0^2} \right], \quad (5b)$$

$$B_{\pm} = \frac{e^{-\lambda_{\pm}t_0}}{\lambda_{+} - \lambda_{-}} \left[\dot{x}_0 - \lambda_{+}x_0 - (\lambda_{+}F_1 + \omega F_2) \sin \omega t_0 - (\lambda_{+}F_2 - \omega F_1) \cos \omega t_0 - (\lambda_{+}G_1 + \Omega G_2) \sin \Omega t_0 - (\lambda_{+}G_2 - \Omega G_1) \cos \Omega t_0 \pm \lambda_{+} \frac{\beta}{\omega_0^2} \right], \quad (5c)$$

with

$$\lambda_{\pm} = \frac{1}{2} \left[-d \pm \sqrt{d^2 - 4\omega_0^2} \right], \quad (5d)$$

$$F_1 = \frac{f(\omega_0^2 - \omega^2)}{(\omega_0^2 - \omega^2)^2 + d^2\omega^2}, \quad F_2 = -\frac{fd\omega}{(\omega_0^2 - \omega^2)^2 + d^2\omega^2}, \quad (5e)$$

$$G_1 = \frac{g(\omega_0^2 - \Omega^2)}{(\omega_0^2 - \Omega^2)^2 + d^2\Omega^2}, \quad G_2 = -\frac{gd\Omega}{(\omega_0^2 - \Omega^2)^2 + d^2\Omega^2}. \quad (5f)$$

In the above solution, the constants A_{\pm} and B_{\pm} are to be evaluated at the initial time $t = t_0$ and reevaluated at other times at which $x = 0$. The initial conditions are $t = t_0 = 0$ with $x(0) = x_0 > 0$, $\dot{x}(0) = \dot{x}_0 = y_0$. With $t_0 = 0$ we calculate A_{+} and B_{+} . Then, we calculate $x(t) = x_{+}(t)$ from Eq. (5a) with time step Δt until $x(t) < 0$. Now, using $x(t - 2\Delta t) > 0$ and $x(t - \Delta t) > 0$, we compute the value of $t = t_c$ (by extrapolation) for which $x(t_c) = 0$. Next, we compute $\dot{x}(t_c)$ by extrapolation. Then, we calculate A_{-} and B_{-} from Eqs. (5b) and (5c), respectively with $t_0 = t_c$, and proceed to calculate $x(t) = x_{-}(t)$ until $x(t) > 0$ and update t_0 , A_{+} and B_{+} and so on.

Case 2: Critical Damping – $d^2 = 4\omega_0^2$

For $d^2 = 4\omega_0^2$, the solution of (1) is given by

$$x_{\pm} = A_{\pm}e^{-dt/2} + tB_{\pm}e^{-dt/2} + F_1 \sin \omega t + F_2 \cos \omega t + G_1 \sin \Omega t + G_2 \cos \Omega t \mp \frac{\beta}{\omega_0^2}, \quad (6)$$

where A_{\pm} and B_{\pm} are to be determined by the values of x_{\pm} and \dot{x}_{\pm} at the time $t = t_0 = 0$ and at other times at which $x = 0$.

Case 3: Underdamping – $d^2 < 4\omega_0^2$

When $d^2 < 4\omega_0^2$, $x_{\pm}(t)$ are given by

$$x_{\pm}(t) = A_{\pm}e^{-dt/2} \cos \tilde{\omega}t + B_{\pm}e^{-dt/2} \sin \tilde{\omega}t + F_1 \sin \omega t + F_2 \cos \omega t + G_1 \sin \Omega t + G_2 \cos \Omega t \mp \frac{\beta}{\omega_0^2}, \quad (7a)$$

where

$$A_{\pm} = \frac{e^{dt_0/2}}{\tilde{\omega}} \left\{ \left(-\frac{d}{2} \sin \tilde{\omega} t_0 + \tilde{\omega} \cos \tilde{\omega} t_0 \right) \left[x_0 - F_1 \sin \omega t_0 - F_2 \cos \omega t_0 - G_1 \sin \Omega t_0 - G_2 \cos \Omega t_0 \mp \frac{\beta}{\omega_0^2} \right], \right. \\ \left. - \sin \tilde{\omega} t_0 \left[\dot{x}_0 - F_1 \omega \cos \omega t_0 + F_2 \omega \sin \omega t_0 - G_1 \Omega \cos \Omega t_0 + G_2 \Omega \sin \Omega t_0 \right] \right\}, \quad (7b)$$

$$B_{\pm} = \frac{e^{dt_0/2}}{\tilde{\omega}} \left\{ \left(\frac{d}{2} \cos \tilde{\omega} t_0 - \tilde{\omega} \sin \tilde{\omega} t_0 \right) \left[x_0 - F_1 \sin \omega t_0 - F_2 \cos \omega t_0 - G_1 \sin \Omega t_0 - G_2 \cos \Omega t_0 \mp \frac{\beta}{\omega_0^2} \right] \right. \\ \left. - \cos \tilde{\omega} t_0 \left[\dot{x}_0 - F_1 \omega \cos \omega t_0 + F_2 \omega \sin \omega t_0 - G_1 \Omega \cos \Omega t_0 + G_2 \Omega \sin \Omega t_0 \right] \right\} \quad (7c)$$

with $\tilde{\omega} = \sqrt{|d^2 - 4\omega_0^2|}$, and F_1 , F_2 , G_1 and G_2 are given by Eqs. (5e) and (5f).

2.2 Contribution to the Response Amplitude by Different Parts of the Solution

We are interested in the effect of the high-frequency driving force on the amplitude of the low-frequency component of the output signal $x(t)$. We treat the amplitude of the high-frequency force as the control parameter. Before reporting the high-frequency induced resonance, we identify the contribution to the response amplitude Q by the various parts of the solution and the term in the solution which gives a dominant contribution to Q .

The response amplitude Q at the low-frequency ω is defined through $Q = \sqrt{Q_c^2 + Q_s^2}/f$ where

$$Q_s = \frac{2}{MT} \int_0^{MT} x(t) \sin \omega t \, dt, \quad (8a)$$

$$Q_c = \frac{2}{MT} \int_0^{MT} x(t) \cos \omega t \, dt. \quad (8b)$$

In Eqs. (8) $T = 2\pi/\omega$ and $M = 1000$.

For convenience we rewrite the solutions $x_{\pm}(t)$ as

$$x_{\pm}(t) = x_{\omega}^{\text{exp}} + x_{\omega_{\pm}}^{\text{imp}} + x_{\text{rem}}, \quad (9a)$$

where

$$x_{\omega}^{\text{exp}} = F_1 \sin \omega t + F_2 \cos \omega t, \quad (9b)$$

$$x_{\omega_{\pm}}^{\text{imp}} = \begin{cases} A_{\pm} e^{\lambda_{\pm} t} + B_{\pm} e^{-\lambda_{\pm} t}, & \text{for } d^2 > 4\omega_0^2 \\ A_{\pm} e^{-dt/2} \cos \tilde{\omega} t + B_{\pm} e^{-dt/2} \sin \tilde{\omega} t, & \text{for } d^2 < 4\omega_0^2 \\ A_{\pm} e^{-dt/2} + B_{\pm} e^{-dt/2}, & \text{for } d^2 = 4\omega_0^2 \end{cases} \quad (9c)$$

$$x_{\text{rem}} = G_1 \sin \Omega t + G_2 \cos \Omega t \mp \frac{\beta}{\omega_0^2}. \quad (9d)$$

In x_{ω}^{exp} , the frequency ω is explicitly present in the argument of the sinusoidal terms. In $x_{\omega_{\pm}}^{\text{imp}}$, the frequency ω appears only in the expressions of A_{\pm} and B_{\pm} , which are updated only when $x(t) = 0$. x_{rem} is independent of ω . We calculate the response amplitudes for $x(t) = x_{\omega}^{\text{exp}}$, $x_{\omega_{\pm}}^{\text{imp}}$ and x_{rem} at the frequency ω and denote them as Q_{exp} , Q_{imp} and Q_{rem} , respectively. We call the response amplitude computed with $x(t) = x_{\pm}(t)$, that is with all the three parts of the solution, as Q . Obviously $Q_{\text{rem}} = 0$ while $Q_{\text{exp}} = \sqrt{F_1^2 + F_2^2}/f$ is independent of the control parameter g . Figure 2 presents the variation of Q , Q_{imp} and Q_{exp} with the control parameter g for the single-well, the double-well and the single-well with a double-hump potentials. In this figure, we observe that in general $Q \neq Q_{\text{exp}} + Q_{\text{imp}}$. However, the variation of Q_{imp} is similar to the variation of Q . The contribution to Q comes from all the terms present in the solution, though some of the terms do not contain ω .

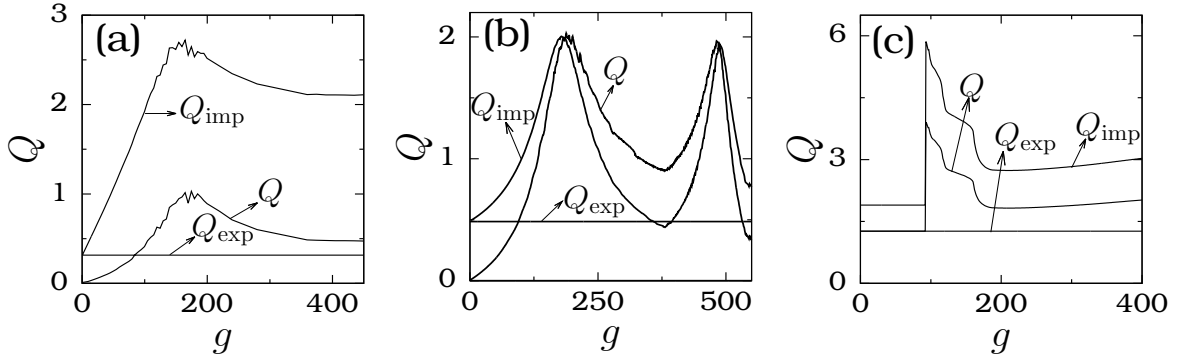


Fig. 2 Variation of Q , Q_{imp} and Q_{exp} with g for the system (1) with (a) single-well potential, (b) single-well with a double-hump potential and (c) double-well potential. The values of the parameters are $d = 0.5$, $f = 0.05$, $\Omega = 20\omega$ and (a) $\omega_0^2 = 1$, $\beta = 0.5$ and $\omega = 2$, (b) $\omega_0^2 = -1$, $\beta = 2$ and $\omega = 2$ and (c) $\omega_0^2 = 1$, $\beta = -1$ and $\omega = 0.5$.

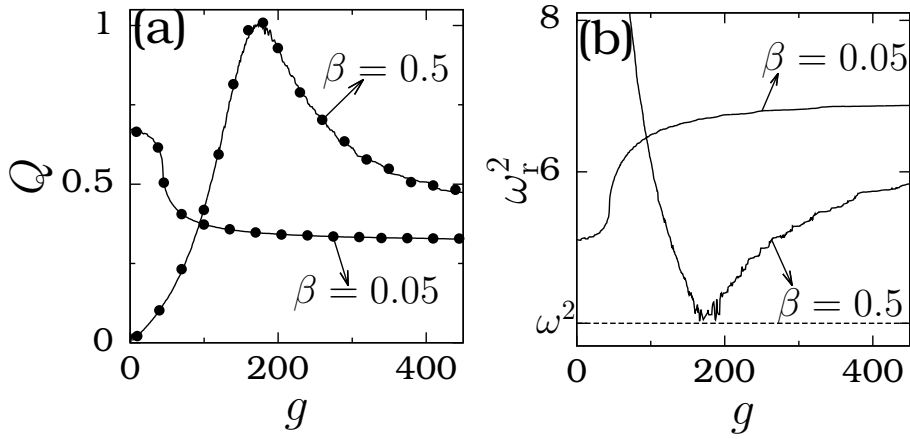


Fig. 3 (a) Variation of Q computed from the analytical solution (7) (continuous curve) and computed from numerical solution (solid circles) with the control parameter g for two values of β for the system (1). The values of the other parameters are $\omega_0^2 = 1$, $d = 0.5$, $f = 0.05$, $\omega = 2$ and $\Omega = 20\omega$. (b) ω_r^2 given by Eq. (11) versus g for two values of β . The horizontal dashed line represents the value of $\omega_r^2 \approx \omega^2$ for which Q becomes a maximum while ω_r^2 becomes a minimum.

3 The System (1) with Single-Well Potential

We consider the system (1) with a single-well potential and with the following choice of parameters $d = 0.5$, $f = 0.05$, $\omega_0^2 = 1$, $\beta > 0$, $\omega = 2$ and $\Omega = 20\omega$. Here $d^2 < 4\omega_0^2$ and the analytical solution of the system is given by Eqs. (7). Figure 3(a) depicts the variation of $Q(\omega)$ computed from the analytical solution (continuous curve) and from the numerical solution obtained by numerically integrating Eq. (1) with a fourth-order Runge–Kutta method. Then, it is used in Eqs. (8) (solid circle) as a function of the control parameter g for two values of β . The values of both the Q 's are almost the same. For $\beta = 0.5$, the response amplitude Q becomes a maximum with the value 1 at $g = 174$. There is no resonance for $\beta = 0.05$.

In order to identify the mechanism of occurrence and nonoccurrence of resonance found for $\beta = 0.5$, we consider the resonant frequency ω_r . For a system driven by the biharmonic force, one can assume that the response of the system essentially consists of a slow motion $X(t, \omega)$ and the fast motion $\psi(t, \Omega t)$ and write $x(t) = X + \psi$. For nonlinear oscillators with polynomial potentials applying a theoretical approach, an approximate equation of motion for the slow variable X and an approximate analytical expression for Q can be obtained

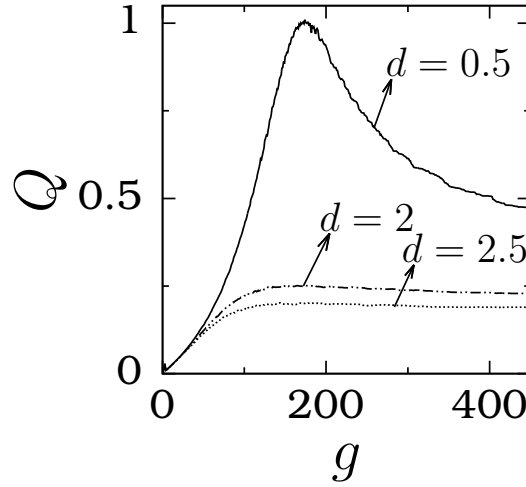


Fig. 4 Q versus g of the system (1) for $d = 0.5$ (underdamped case), $d = 2$ (critical damped case) and $d = 2.5$ (overdamped case) with $\omega_0^2 = 1$, $\beta = 0.5$, $f = 0.05$, $\omega = 2$ and $\Omega = 20\omega$.

[23,26]. The general form of the analytical expression of Q is given by

$$Q = \frac{1}{\sqrt{(\omega_r^2 - \omega^2)^2 + d^2\omega^2}}, \tag{10}$$

where ω_r is the resonant frequency of oscillation of the linearized equation of motion of the slow variable X . ω_r is generally a function of the parameters ω_0^2 , β , g and Ω , that is $\omega_r^2 = F(\omega_0^2, \beta, g, \Omega)$ [23, 26]. The form of F depends on the form of the nonlinearity present in the system.

Assuming the response amplitude Q in the form of Eq. (10), we write

$$\omega_r^2 = \omega^2 + \sqrt{\frac{1}{Q^2} - d^2\omega^2} \tag{11}$$

and compute ω_r^2 corresponding to the Fig. 3(a). The result is presented in Fig. 3(b). In this figure the horizontal dashed line represents the value of $\omega_r^2 = \omega^2$. For $\beta = 0.5$ as g increases from a small value, the quantity ω_r^2 decreases from a large value $> \omega^2$. Consequently, Q increases from a small value. At a value of $g = 174$, $\omega_r^2 \approx \omega^2$ and according to Eq. (10) $Q \approx 1/d\omega = 1$. In Fig. 3(a) at resonance $Q \approx 1$. This implies that for the system (1) one can introduce a resonant frequency (its analytical expression for the system (1) is not known) associated with the slow variable and resonance occurs when either ω_r matches with the frequency ω of the low-frequency input signal or the quantity $\omega_r^2 - \omega^2$ becomes a nonzero minimum. We denote the value of g at which resonance occurs as g_{VR} . For $g > g_{VR}$, Q decreases but not decays to zero. In Fig. 3(b) ω_r^2 matches with ω^2 at only one value of g and Q becomes maximum at one value of g . For $\beta = 0.05$ $\omega_r^2 \neq \omega^2$ (refer to Fig. 3(b)) when g is varied and there is no resonance.

In the above, we considered the choice $d = 0.5$ and $\omega_0^2 = 1$. For this choice $d^2 = 0.25 < \omega_0^2 = 1$ (underdamped case) and the analytical solution used is given by Eqs. (7). In Fig. 4, we plot Q versus g for the overdamped case with $d = 2.5$ and the critical damping case with $d = 2$ together with $d = 0.5$ (underdamped case). The analytical solutions used for $d = 0.5$, 2 and 2.5 are given by the Eqs. (5), (6) and (7), respectively. According to Eq. (10) the effect of damping is to change the value of Q , however, it does not affect the value of g_{VR} at which the resonance occurs. Moreover, for $d = 0.5$, 2 and 2.5 the value of Q at resonance are expected to be 1, 0.25 and 0.2, respectively. Same results are found in Fig. 4.

Next, we present the effect of β on vibrational resonance. Q is calculated for $g \in [0, 500]$ and $\beta \in [0, 2]$. Figure 5 shows the response amplitude profile as a function of g and β . For $\beta \leq 0.05$, there is no resonance and

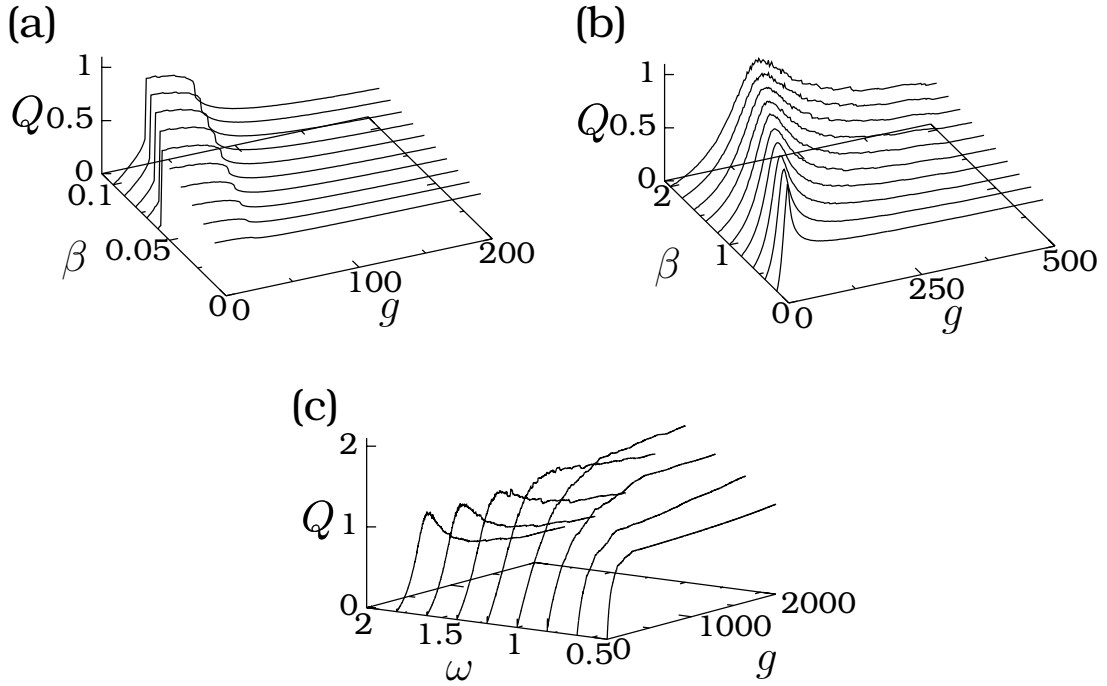


Fig. 5 Variation of Q with g for selected values of $\beta \in [0, 2]$ of the system (1) with $\omega_0^2 = 1$, $d = 0.5$, $f = 0.05$, $\omega = 2$ and $\Omega = 20\omega$.

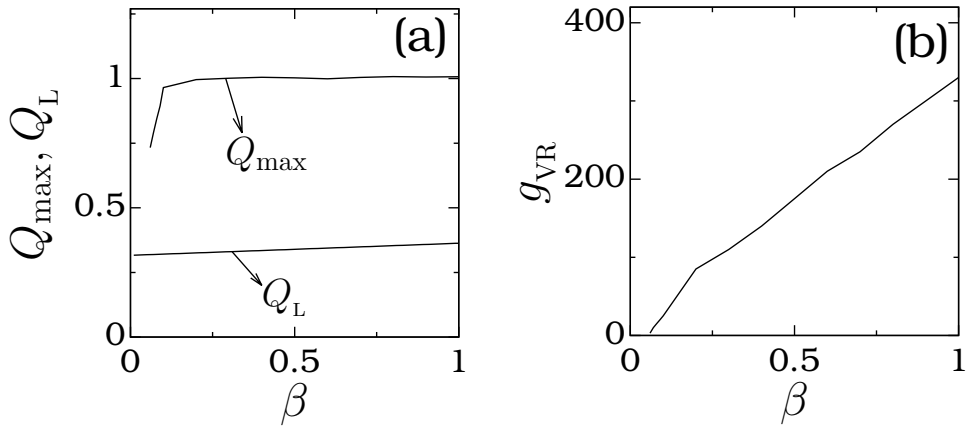


Fig. 6 Plot of (a) Q_{\max} and Q_L and (b) g_{VR} as a function of β for the system (1) with $\omega_0^2 = 1$, $d = 0.5$, $f = 0.05$, $\omega = 2$ and $\Omega = 20\omega$.

the value of Q at $g = 0$ is > 0 . A single resonance occurs for $\beta > 0.05$. In Fig. 5 we can clearly observe that for $\beta > 0.05$, $Q(g = 0) = 0$. For $\beta > 0.05$ in the absence of the high-frequency force $g \cos \Omega t$ and driven by the low-frequency force $f \cos \omega t$ the long time evolution of the system is not oscillatory. The system exhibits amplitude death and $x(t) \rightarrow 0$ as $t \rightarrow \infty$. A periodic oscillation with period $2\pi/\omega$ is induced by the high-frequency driving force. Another important observation is that Q does not decay to zero after passing through the resonance. Q attains a nonzero saturation value for sufficiently large values of g . Such a response dynamics is previously found in pendulum and Morse oscillator systems [33, 40]. In many oscillators Q is found to decay to zero for large values of g . We denote the limiting value of Q (in the limit of $g \rightarrow \infty$) as Q_L . The variations of Q_{\max} (the value of Q at resonance), Q_L and g_{VR} with β are shown in Fig. 6. Except for very small values of β , $Q_{\max} \approx 1$ ($= 1/d\omega$)

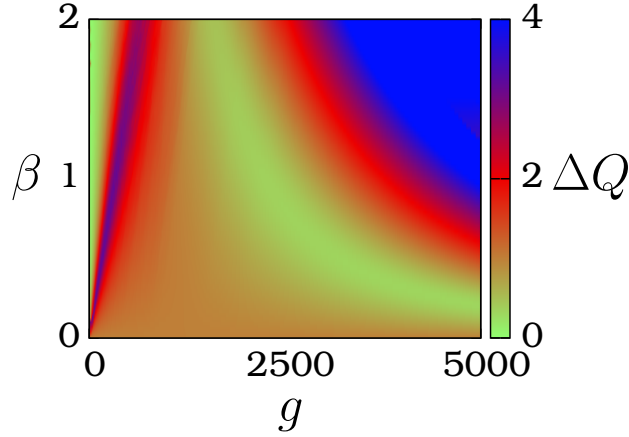


Fig. 7 Color code plot of $\Delta Q (= Q_S/Q_D)$ as a function of the parameters β and g for the single-well potential case of the system (efe1) and the Duffing oscillator.

while Q_L and g_{VR} increase linearly with β .

It is noteworthy to compare the dependence of Q on the parameters of the system (1) and the Duffing oscillator with a single-well potential. For the Duffing oscillator, a theoretical treatment of vibrational resonance analysis gives [26]

$$Q_D = \frac{1}{\sqrt{(\omega_f^2 - \omega^2)^2 + d^2\omega^2}}, \quad \omega_f^2 = \omega_0^2 + \frac{3\beta g^2}{4\Omega^4}, \quad (12a)$$

and

$$g_{VR} = \left[\frac{2\Omega^4}{3\beta} (\omega^2 - \omega_0^2) \right]^{1/2}. \quad (12b)$$

From Eqs. (12) for the Duffing oscillator system we infer the following:

- (i) Vibrational resonance occurs only for $\omega^2 > \omega_0^2$.
- (ii) There is always one resonance for $\beta > 0$ and $\omega^2 > \omega_0^2$.
- (iii) $Q_D \rightarrow 0$ as $g \rightarrow \infty$.
- (iv) g_{VR} decreases with increase in β .
- (v) $Q_{D,max} = 1/d\omega$.

For $\omega^2 < \omega_0^2$ there is no resonance and Q decreases monotonically from a nonzero value with increase in the value of g and approaches 0 in the limit of $g \rightarrow \infty$. For the system (1) the following results are observed:

- (i) For each fixed value of ω with $\omega^2 > \omega_0^2$, resonance occurs for β values above a critical value.
- (ii) Q_S (Q of the system (1)) does not decay to zero as $g \rightarrow \infty$, but approaches a limiting value.
- (iii) g_{VR} increases with β (as shown in Fig. 6(b)).
- (iv) $Q_{S,max} \approx 1/d\omega$ except for small values of β (refer Fig. 6(a)).
- (v) For $\omega^2 < \omega_0^2$, as g increases from a small value, the response amplitude Q increases from a small value and then attains a saturation displaying a sigmoidal type variation (see Fig. 5(c)). In order to compare the values of Q of the two systems, we compute the quantity $\Delta Q = Q_S/Q_D$. Figure 7 presents the dependence of ΔQ on β and g .

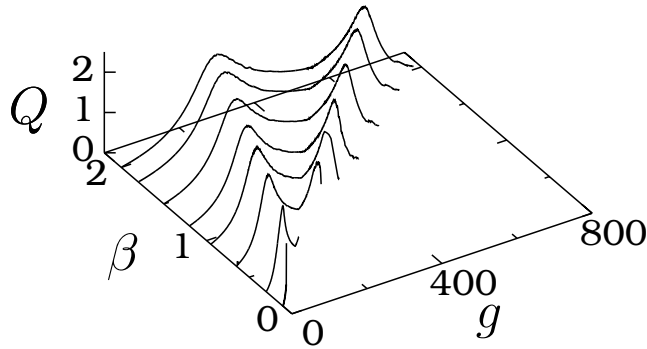


Fig. 8 The effect of β on Q computed from the analytical solution for the system (1) with the double-hump potential. The values of the parameters are $d = 0.5$, $\omega_0^2 = -1$, $f = 0.05$, $\omega = 1$ and $\Omega = 20\omega$.

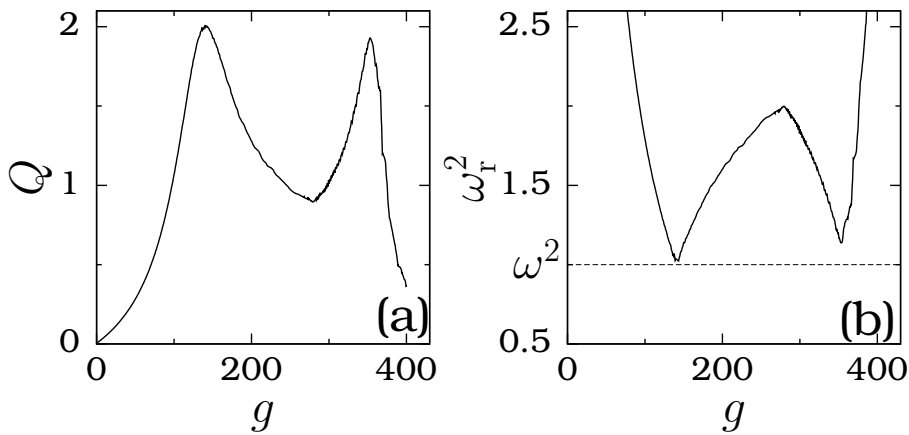


Fig. 9 (a) Variation of Q with the control parameter g of the system (1) with the double-hump single-well potential. Here $d = 0.5$, $\omega_0^2 = -1$, $\beta = 1$, $f = 0.05$, $\omega = 1$ and $\Omega = 20\omega$. (b) ω_r^2 versus g corresponding to the subplot (a).

4 Single-Well with a Double-Hump Potential

The shape of the potential of the system (1) for $\omega_0^2 < 0$ and $\beta > 0$ is the single-well with a double-hump as shown in Fig. 1(b). For our analysis of the vibrational resonance in (1), we fix $\omega_0^2 = -1$, $\beta > 0$, $d = 0.5$, $f = 0.05$, $\omega = 1$ and $\Omega = 20\omega$. Figure 8 depicts the effect of β on Q computed from the analytical solution. The effect of β is clearly seen in this figure. There are three notable effects of β :

- (i) $Q(\omega) = 0$ when $g = 0$, even though the system is driven by a periodic force.
- (ii) For $\beta < \beta_{c1} = 0.104$, there is no resonance.
- (iii) For $\beta_{c1} < \beta < \beta_{c2} = 0.39$, it displays only one resonance. There are two resonances for $\beta > \beta_{c2}$.
- (iv) For each fixed value of β , as g increases, the maximum and minimum values of $x(t)$ increase. Above a critical value of g , $x(t)$ crosses the barriers at $x_{\pm} = \pm\beta/|\omega_0^2|$. Since $V_S(x) \rightarrow -\infty$ for $x \rightarrow \pm\infty$, the solution $x(t) \rightarrow \pm\infty$. The solution $x(t)$ is now unbounded and hence the response amplitude curve terminates at a value of g . We denote the value of g below which $x(t)$ is bounded as g_b . This critical value of g increases for increasing values of β .

In order to describe the occurrence of resonance in the system (1) for the double-hump single-well potential case, we plot in Fig. 9 Q and ω_r^2 versus g for $\beta = 1$. Q is maximum at $g = 141$ with $Q_{\max} = 2$ and at $g = 352$ with $Q_{\max} = 1.93$. When $\beta = 0.5$, Q is maximum at only one value of $g (= 67)$ with $Q_{\max} = 2$. Furthermore, $x(t)$

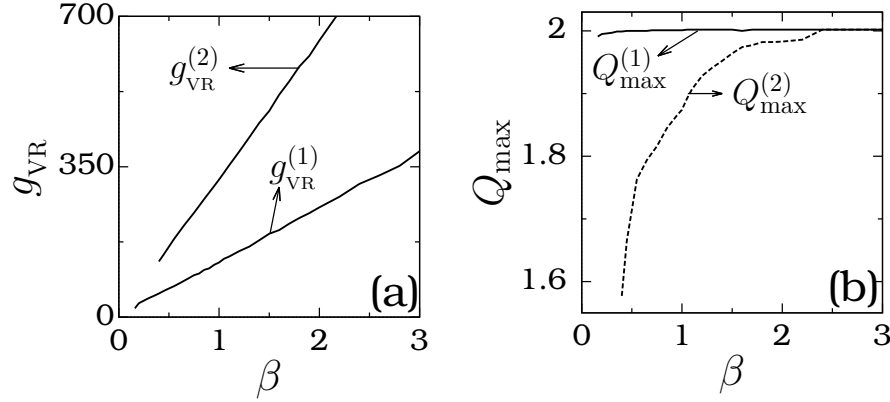


Fig. 10 Dependence of $g_{\text{VR}}^{(1)}$, $g_{\text{VR}}^{(2)}$, $Q_{\text{max}}^{(1)}$ and $Q_{\text{max}}^{(2)}$ with the parameter β for the system (1) with a double-hump single-well potential.

becomes unbounded for $g > g_b = 170$. When g increases from a small value, then ω_f^2 exhibits a finite number of oscillations. Moreover, Q becomes a maximum (minimum) when ω_f^2 attains locally a minimum (maximum) value. At $g = g_{\text{VR}}^{(1)} = 147$, ω_f^2 becomes a minimum with the value ω^2 and hence Q becomes a maximum with the value $Q_{\text{max}}^{(1)} = 1/d\omega = 2$. The second resonance occurs at $g = g_{\text{VR}}^{(2)} = 352$. At this value of g , the quantity ω_f^2 is locally a minimum, but with a value $\neq \omega^2$ and hence $Q_{\text{max}}^{(2)} \neq 2$. That is, when the resonance is due to the matching of ω_f^2 with ω^2 of the low-frequency force then $Q_{\text{max}} = 1/d\omega$. If the resonance is due to the local minimization of ω_f^2 without matching with ω^2 then $Q_{\text{max}} < 1/d\omega$.

The values of $g_{\text{VR}}^{(1)}$, $g_{\text{VR}}^{(2)}$, $Q_{\text{max}}^{(1)}$ and $Q_{\text{max}}^{(2)}$ are computed for $\beta \in [\beta_{c1}, 2]$. Figure 10 depicts the variation of these quantities with β . Both $g_{\text{VR}}^{(1)}$ and $g_{\text{VR}}^{(2)}$ vary linearly with β , but with different rate. The width between $g_{\text{VR}}^{(1)}$ and $g_{\text{VR}}^{(2)}$ increases with β . In Fig. 10(a), $Q_{\text{max}}^{(1)} \approx 2$ implying that the first resonance is due to $\omega_f^2 \approx \omega^2$. For $\beta > \beta_{c2}$, the response amplitude $Q_{\text{max}}^{(2)}$ increases and approaches $Q_{\text{max}}^{(2)}$ for $\beta \gg 1$.

Next, we compare the vibrational resonance of the system (1) with that of the Duffing oscillator. For $\omega_0^2 < 0$ and $\beta > 0$, the potential V_S is a single-well with a double-hump while the shape of V_D is a double-well. V_D is a double-hump single-well form for $\omega_0^2 < 0$ and $\beta > 0$. For the system (1), we choose $\omega_0^2 < 0$ and $\beta > 0$, while for the Duffing oscillator we choose $\omega_0^2 > 0$ and $\beta < 0$. For the Duffing oscillator an approximate theoretically obtained response amplitude is given by Eq. (12a), where $\omega_f^2 = \omega^2 - \beta g^2/2\Omega^2$. Matching of ω_f^2 with ω^2 yields

$$g_{\text{VR}} = \sqrt{\frac{2\Omega^4 (\omega_0^2 - \omega^2)}{3|\beta|}}, \quad \omega^2 < \omega_0^2. \quad (13)$$

Equation (13) implies that at most only one resonance is possible in the Duffing oscillator, while in the system (1) for a range of values of β two resonances take place (see Figs. 8 and 10). In both systems Q_{max} at the first resonance is always $1/d\omega$.

The potentials V_S and V_D can be compared in terms of the depth of the potential well and the location x_{\pm}^* at which the potentials are locally maximum. The x_{\pm}^* are the x -components of the unstable equilibrium points of the system (1) and the Duffing oscillator in absence of the driving force. The depths of the potential wells of V_S and V_D , denoted as d_S and d_D , respectively, are given by

$$d_S = \left| \frac{\beta^2}{2\omega_0^2} \right|, \quad d_D = \left| \frac{\omega_0^4}{4\beta} \right|. \quad (14a)$$

The x^* of the two systems are

$$x_{\pm,S}^* = \pm \left| \frac{\beta}{\omega_0^2} \right|, \quad x_{\pm,D}^* = \pm \sqrt{\left| \frac{\omega_0^2}{\beta} \right|}. \quad (14b)$$

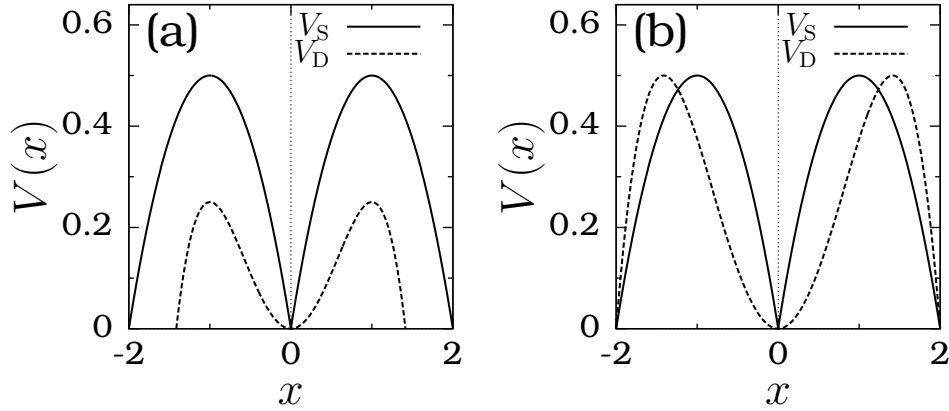


Fig. 11 Plot of V_S and V_D with (a) $x_S^* = x_D^*$ and (b) $d_S = d_D$. In (a) $\omega_0^2 = -1$, $\beta = 1$ for V_S and $\omega_0^2 = 1$, $\beta = -1$ for V_D . In (b) $\omega_0^2 = 1$, $\beta = -1$ for V_S and $\omega_0^2 = 1$, $\beta = -2$.

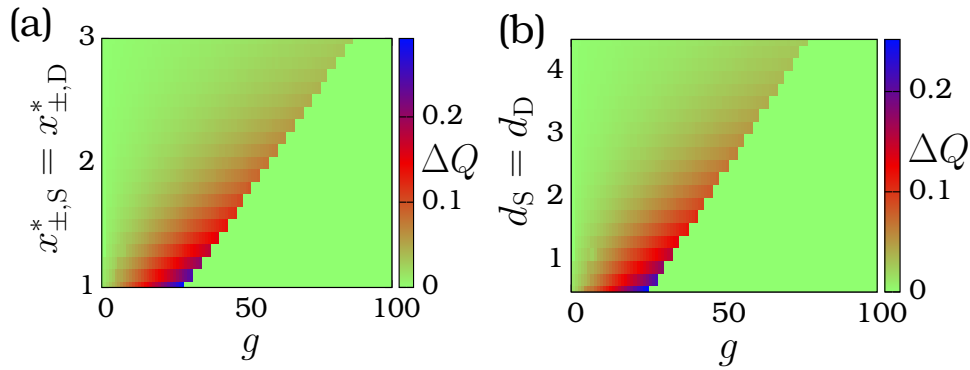


Fig. 12 Color code representation of ΔQ ($= Q_S/Q_D$) as a function of g and (a) $x_{\pm,S}^* = x_{\pm,D}^*$ and (b) $d_S = d_D$.

Figures 11(a) and (b) show V_S and V_D with $x_{\pm,S}^* = x_{\pm,D}^*$ and $d_S = d_D$, respectively. We computed Q_S and Q_D as a function of g and (i) $x_{\pm,S}^* = x_{\pm,D}^*$ and (ii) $d_S = d_D$. Then $\Delta Q = Q_S/Q_D$ is calculated. Figure 12 presents the result.

5 Double-Well Potential

The potential of the system (1) becomes of a double-well form for $\omega_0^2 > 0$ and $\beta < 0$. We fix the values of the parameters as $d = 0.5$, $\omega_0^2 = 1$, $f = 0.05$, $\omega = 0.5$ and $\Omega = 20\omega$. For $d = 0.5$ and $\omega_0^2 = 1$ the system is underdamped in absence of an external periodic force. The analytical solution of the forced system (1) for the underdamped case is given by Eq. (7). Figures 13(a) and (b) present the dependence of the response amplitude $Q(\omega)$ as a function of g for a range of fixed values of β for $\omega = 0.5$ and $\omega = 1.5$, respectively. In Fig. 13(a) we observe that for each fixed value of $\beta < 0$, the response amplitude Q is a constant for g values less than a critical value g_c . This critical value varies with β . As g passes through g_c , the response amplitude increases, reaches a maximum, decreases with further increase in g and then approaches a constant value. In Fig. 13(a), we can clearly notice the effect of β on the response profile. The variations of g_{VR} , Q_{max} and Q_L with the parameter β are presented in Fig. 14. g_{VR} increases linearly with increases in $|\beta|$. Except for β values near zero, Q_{max} becomes 4 ($= 1/d\omega$) for $\beta < 0$. Q_L remains at the value of 1.25.

In order to compare the response amplitudes of the signum nonlinearity system and the Duffing oscillator, we consider the location of the local minima and the depth of the potential wells. They are given by the Eqs. (14a) and (14b). Figure 15 presents the dependence of ΔQ ($= Q_S/Q_D$), where Q_S and Q_D are the response

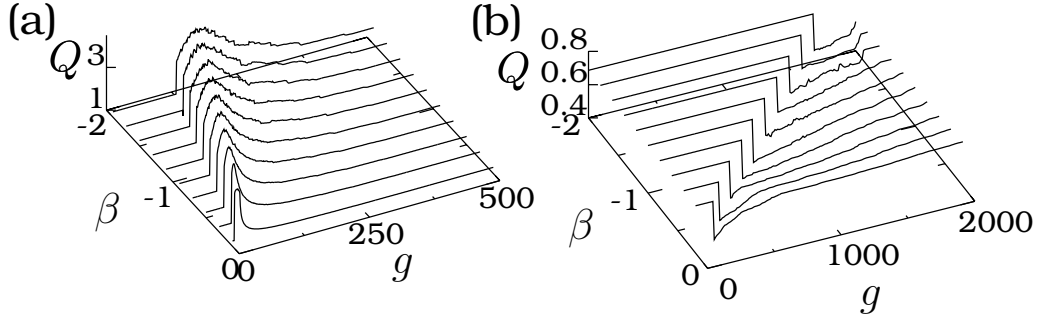


Fig. 13 Q as a function of g and β for the double-well potential case of the system (1). The value of the other parameters are $d = 0.5$, $f = 0.05$, $\omega_0^2 = 1$, $\Omega = 20\omega$. (a) $\omega = 0.5$ and (b) $\omega = 1.5$.

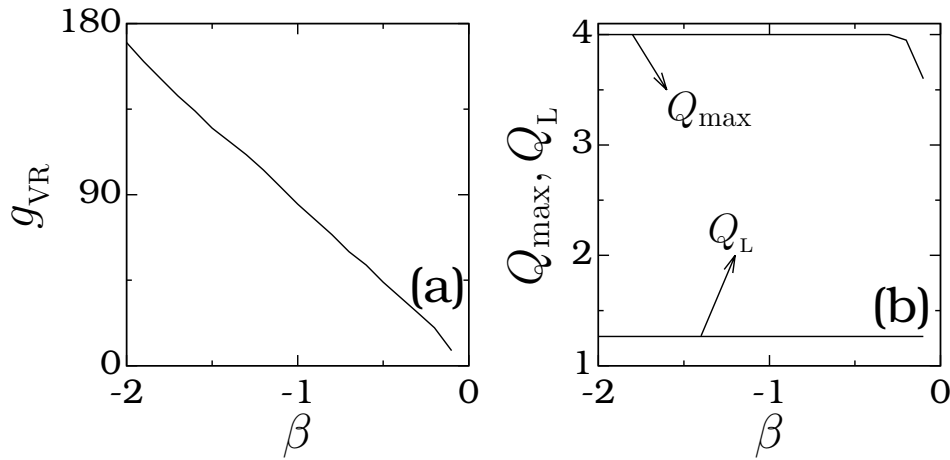


Fig. 14 (a) g_{VR} versus β and (b) Q_{max} and Q_L versus β for the double-well potential case of the system (1).

amplitude of the system (1) and the Duffing oscillator, as a function of the parameter g and the cases of $d_S = d_D$ and $x_{\pm,S}^* = x_{\pm,D}^*$.

For the double-well potential Duffing oscillator ($\omega_0^2 < 0$, $\beta > 0$) the approximate analytical expression for Q is given by Eq. (12a) with

$$\omega_r^2 = -|\omega_0^2| + 3\beta x^{*2}, \quad x^* = \pm \sqrt{-\frac{c_1}{\beta}}, \quad 0, \quad c_1 = -|\omega_0^2| + \frac{3\beta g^2}{2\Omega^4}. \quad (15)$$

Resonance occurs at

$$g_{VR}^{(1)} = \left[\frac{\Omega^4}{3\beta} (2|\omega_0^2| - \omega^2) \right]^{1/2}, \quad 2|\omega_0^2| > \omega^2 \quad (16a)$$

and

$$g_{VR}^{(2)} = \left[\frac{2\Omega^4}{3\beta} (|\omega_0^2| + \omega^2) \right]^{1/2}. \quad (16b)$$

$g_{VR}^{(1)}$ and $g_{VR}^{(2)}$ are obtained from $\omega_r^2 = \omega^2$ with $x^* = \pm \sqrt{-c_1/\beta}$ and 0, respectively. Two resonances occur for $2|\omega_0^2| > \omega^2$ while one resonance for $2|\omega_0^2| < \omega^2$. In Fig. 13(a) Q is plotted for the system (1), where $\omega_0^2 = 1$ and $\omega = 0.5$ so that $2|\omega_0^2| > \omega^2$. We observe only one resonance. In contrast to this for $2|\omega_0^2| > \omega^2$ the Duffing oscillator displays two resonances. For $2|\omega_0^2| < \omega^2$ there is no resonance for the signum nonlinear system as shown in Fig. 13(b) for $\omega_0^2 = 1$ and $\omega = 1.5$. For this case the Duffing oscillator admits one resonance.

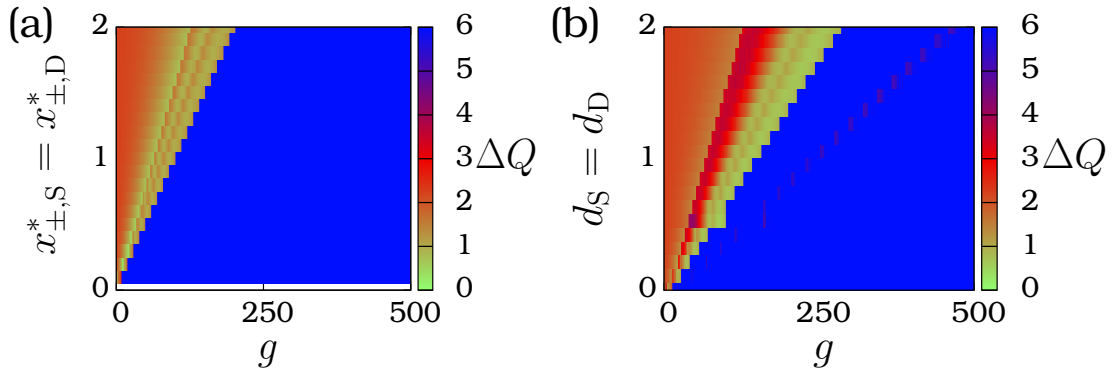


Fig. 15 Color code representation of $\Delta Q (= Q_S/Q_D)$ as a function of g and (a) $x_{\pm,S}^* = x_{\pm,D}^*$ and (b) $d_S = d_D$.

In the Duffing oscillator both $g_{VR}^{(1)}$ and $g_{VR}^{(2)}$ decrease with increase in the value of β . In contrast to this, as shown in Fig. 14(a) for the system (1), g_{VR} increases with increase in the value of $|\beta|$. In both systems, at resonance $Q_{max} = 1/d\omega$ except for $|\beta| \ll 1$ in the system (1). Further, in the system (1) $Q_L \neq 0$ and becomes independent of β (Fig. 14(b)) while in the Duffing oscillator $Q \rightarrow 0$ as $g \rightarrow \infty$.

6 Conclusions

In the present paper the phenomenon of vibrational resonance is analysed in a piecewise linear system. An important and interesting significance of this system is that it possesses an exact analytical solution in the presence of an external biharmonic force. As the potentials of the system (1) and the Duffing oscillator have similar shapes, we have compared the features of vibrational resonance in these systems. Even though the exact analytical solution of the system (1) is known, determination of an analytical expression for its response amplitude is not feasible. On the other hand, without determining the analytical solution, an analytical expression for the response amplitude is obtained for the Duffing oscillator through a theoretical approach. In the Duffing oscillator, the resonance is always due to the matching of the resonant frequency ω_r with the frequency ω of the external driving force. In the system (1) resonance is due to either $\omega_r = \omega$ or local minimization of ω_r . In the Duffing oscillator $Q \rightarrow 0$ as $g \rightarrow \infty$, while in the system (1) $Q_L \neq 0$. In the system (1) g_{VR} always increases with increase in the value of the parameter $|\beta|$ for all the three physically interesting types of potential. In contrast to this, in the Duffing oscillator g_{VR} always decreases with increases in $|\beta|$. For a certain range of values of ω_0^2 and β , the system (1) exhibits a sigmoid type variation of Q with the control parameter g . Such a type of response is not realized in the Duffing oscillator system. When $g = 0$ and $f \neq 0$, the response amplitude $Q(\omega)$ is always nonzero in the Duffing oscillator. That is, the output of the system is oscillating and contains the frequency ω . In contrast to this, in the system (1) for a wide range of values of the parameters of the system, oscillation death occurs for $f \neq 0$ and $g = 0$ (see Figs. 5(b) and 8). The addition of a high-frequency force induces oscillations containing the frequency ω . A detailed investigation of vibrational resonance in other piecewise linear systems may bring out some more other common features of resonance in piecewise linear systems over the nonlinear systems such as the Duffing oscillator and quintic oscillator.

7 Acknowledgments

KA acknowledges the support from University Grants Commission (UGC), India in the form of UGC-Rajiv Gandhi National Fellowship. MAFS acknowledges financial support from the Spanish Ministry of Economy and Competitivity under Project No. FIS2013-40653-P.

References

- [1] Moon, F.C. and Holmes, P.J. (1979) A magnetoelastic strange attractor, *Journal of Sound and Vibration*, **65**, 275-296.
- [2] Lakshmanan, M. and Rajasekar, S. (2003) *Nonlinear Dynamics: Integrability, Chaos and Patterns*, Springer-Verlag: New York.
- [3] Fortuna, L., Frasca, M. and Xibilia, M.G. (2009) *Chua's Circuit Implementations: Yesterday, Today and Tomorrow*, World Scientific, Singapore.
- [4] Kilic, R. (2010) *A Practical Guide for Studying Chua's Circuits*, World Scientific, Singapore.
- [5] Chua, L.O., Desoer, C.A. and Kuh, E.S. (1987) *Linear and Nonlinear Circuits*, McGraw-Hill, Singapore.
- [6] Lakshmanan, M. and Murali, K. (1996) *Chaos in Nonlinear Oscillators: Controlling and Synchronization*, World Scientific, Singapore.
- [7] Chua, L.O. (1977) Section-wise piecewise-linear functions: Canonical representation, properties, and applications *Proceedings of IEEE*, **65**, 915-926.
- [8] Bernardo, M., Budd, C., Champneys, A.R. and Kowalczyk, P. (2008) *Piecewise-smooth Dynamical Systems: Theory and Applications*, Springer-Verlag: New York.
- [9] De Feo, O. and Storace, M. (2007) Piecewise-linear identification of nonlinear dynamical systems in view of their circuit implementations *Circuits and Systems I: Regular Papers, IEEE Transactions*, **54**, 1542-1554.
- [10] Li, C., Sprott, J.C., Thio, W. and Zhu, H. (2014) A new piecewise linear hyperchaotic circuit, *IEEE Transactions on Circuits and Systems-II*, **61**, 977-981.
- [11] Lowe, G.K. and Zohdy, G.K. (2010) Modeling nonlinear systems using multiple piecewise linear equations, *Nonlinear Analysis: Modelling and Control*, **15**, 451-458.
- [12] Kominis, Y. and Bountis, T. (2010) Analytical solutions with piecewise linear dynamics, *International Journal of Bifurcation and Chaos*, **20**, 509-518.
- [13] Grantham, W.J. and Lee, B. (1993) A chaotic limit cycle paradox, *Dynamics and Control*, **3**, 157-171.
- [14] Sprott, J.C. (2000) Simple chaotic systems and circuits, *American Journal of Physics*, **68**, 758-763.
- [15] Gottlieb, H.P.W. and Sprott, J.C. (2001) Simplest driven conservative chaotic oscillator, *Physics Letters A*, **291**, 385-388.
- [16] Danca, M.-F. and Codreanu, S. (2002) On a possible approximation of discontinuous dynamical systems, *Chaos, Solitons and Fractals*, **13**, 681-691.
- [17] Hai, D.D. (2007) On a class of quasilinear systems with sign-changing nonlinearities, *Journal of Mathematical Analysis and Applications*, **334**, 965-976.
- [18] Cortes, J. (2008) Discontinuous dynamical systems, *Control Systems, IEEE*, **28**, 36-73.
- [19] Sun, K. and Sprott, J.C. (2010) Periodically forced chaotic system with signum nonlinearity, *International Journal of Bifurcation and Chaos*, **20**, 1499-1508.
- [20] Zhang, J., Zhang, Y., Ali, W. and Shieh, L. (2011) Linearization modeling for non-smooth dynamical systems with approximated scalar sign function, *Decision and Control and European Control Conference (CDC-ECC), 50th IEEE Conference*, 5205-5210.
- [21] Cheng, Z. and Li, C. (2015) Shooting method with sign-changing nonlinearity, *Nonlinear Analysis*, **114**, 2-12.
- [22] Sun, K., Li-kun, A.D.D., Dong, Y., Wang, H. and Zhong, K. (2013) Multiple coexisting attractors and hysteresis in the generalized Ueda oscillator, *Mathematical Problems in Engineering*, **2013**, 1-7.
- [23] Landa, P.S. and McClintock, P.V.E. (2000) Vibrational resonance, *Journal of Physics A: Mathematical and General*, **33**, L433-L438.
- [24] Gitterman, M. (2001) Bistable oscillator driven by two periodic fields, *Journal of Physics A: Mathematical and General*, **34**, L355-L357.
- [25] Ullner, E., Zaikin, A., Garcia-Ojalvo, J., Bascones, R. and Kurths, J. (2003) Vibrational resonance and vibrational propagation in excitable systems, *Physics Letters A*, **312**, 348-354.
- [26] Blechman, I.I. and Landa, P.S. (2004) Conjugate resonances and bifurcations in nonlinear systems under biharmonic excitation, *International Journal of Non-Linear Mechanics*, **39**, 421-426.
- [27] Chizhevsky, V.N. and Giacomelli, G. (2008) Vibrational resonance and the detection of aperiodic binary signals, *Physical Review E*, **77**, 051126-1-7
- [28] Chizhevsky, V.N. (2008) Analytical study of vibrational resonance in an overdamped bistable oscillator, *International Journal of Bifurcation and Chaos*, **18**, 1767-1774.
- [29] Jeyakumari, S., Chinnathambi, V., Rajasekar, S. and Sanjuan, M.A.F. (2009) Single and multiple vibrational resonance in a quintic oscillator with monostable potentials, *Physical Review E*, **80**, 046608-1-7.
- [30] Jeyakumari, S., Chinnathambi, V., Rajasekar, S. and Sanjuan, M.A.F. (2009) Analysis of vibrational resonance in a quintic oscillator, *Chaos*, **19**, 043128-1-8.
- [31] Deng, B., Wang, J., Wei, X., Tsang, K.M. and Chan W.L. (2010) Vibrational resonance in neuron populations, *Chaos*, **20**, 013113-1-7.
- [32] Jeevarathinam, C., Rajasekar, S. and Sanjuan, M.A.F. (2011) Theory and numerics of vibrational resonance in Duffing

- oscillators with time-delayed feedback, *Physical Review E*, **83**, 066205-1-12.
- [33] Rajasekar, S., Abirami, K. and Sanjuan, M.A.F. (2011) Novel vibrational resonance in multistable systems, *Chaos*, **21**, 033106-1-7.
- [34] Chizhevsky, V.N., Smeu, E. and Giacomelli, G. (2003) Experimental evidence of vibrational resonance in an optical system, *Physical Review Letters*, **91**, 220602-1-4.
- [35] Ghosh, S. and Ray, D.S. (2015) Optical Bloch equations in a bichromatic field; vibrational resonance, *The European Physical Journal B*, **88**, 1-5.
- [36] Ghosh, S. and Ray, D.S. (2013) Nonlinear vibrational resonance, *Physical Review E*, **88**, 042904-1-6.
- [37] Daza, A., Wagemakers, A. and Sanjuan M.A.F. (2013) Strong sensitivity of the vibrational resonance induced by fractal structure, *International Journal of Bifurcation and Chaos*, **23**, 1350129-1350136.
- [38] Rajasekar, S., Used, J., Wagemakers, A. and Sanjuan, M.A.F. (2012) Vibrational resonance in biological nonlinear maps, *Communication on Nonlinear Science and Numerical Simulation*, **17**, 3435-3445.
- [39] Wang, C., Yang, K. and Qu, S. (2014) Vibrational resonance in a discrete neuronal model with time delay, *International Journal of Modern Physics B*, **28**, 1450103-112.
- [40] Abirami, K., Rajasekar, S. and Sanjuan, M.A.F. (2013) Vibrational resonance in the Morse oscillator, *Pramana Journal of Physics*, **81**, 127-141.